

# Deep-Circuit QAOA

Gereon Koßmann,<sup>1, a)</sup> Lennart Binkowski,<sup>1, b)</sup> Lauritz van Luijk,<sup>1</sup> Timo Ziegler,<sup>1, 2, c)</sup> and René Schwonnek<sup>1, d)</sup>

<sup>1)</sup>*Institut für Theoretische Physik, Leibniz Universität Hannover*

<sup>2)</sup>*Volkswagen AG, Group Innovation*

Despite its popularity, several empirical and theoretical studies suggest that the quantum approximate optimization algorithm (QAOA) has issues in providing a substantial practical advantage. So far, those findings mostly account for a regime of few qubits and shallow circuits. In this work we extend on this by investigating the perspectives of QAOA in a regime of deep quantum circuits.

Due to a rapidly growing range of classical control parameters, we consider local search routines as the characteristic class of variation methods for this regime. The behaviour of QAOA with local search routines can be best analyzed by employing Lie theory. This gives a geometrically nice picture of optimization landscapes in terms of vector and scalar fields on a differentiable manifold. Our methods are clearly borrowed from the field of optimal control theory.

In the limit of asymptotic circuits we find that a generic QAOA instance has many favourable properties, like a unique local minimum. For deep but not close to asymptotically deep circuits many of those nice properties vanish. Saddle points turn into effective local minima, and we get a landscape with a continuum of local attractors and potentially exponentially many local traps. Our analysis reveals that statistical distribution properties of traps, like amount, sizes, and depths, can be easily accessed by solely evaluating properties of the classical objective function. As a result we introduce performance indicators that allow us to assess if a particular combinatorial optimization problem admits a landscape that is favourable for deep circuit QAOA.

Even though we see that there is no free lunch on general instances, certain problem classes like random QUBO, MAXCUT on 3-regular graphs, or a very unbalanced MAX- $k$ -SAT have a chance to perform not too bad in the deep circuit regime.

## I. INTRODUCTION

Within recent years, *variational quantum algorithms* (VQAs)<sup>1</sup> have become the focus of a significant amount of research. The intuitive idea of this class of algorithms is to use classical optimization routines, which could for example include methods from machine learning, in order to variationally combine small building blocks of quantum circuits into bigger ones that may give good solutions to difficult problems.

Due to its elegant simplicity, the *quantum approximate optimization algorithm* (QAOA)<sup>2</sup> is one of the most prominent types of algorithms from the growing family of VQAs. It was designed to tackle the class of *combinatorial optimization problems* (see Section II). This class includes for example problems like MAXCUT, MAX- $k$ -SAT, or TSP, and can in general be considered to be of practical relevance for real world applications. Algorithms for non-trivial instances of these can already be implemented on systems with only a few dozen of qubits; e.g. [3] (figure 4) use up to 23 qubits. This is why QAOA attracted, beyond a pure academic interest, also a lot of attention by several of the first commercial providers of quantum software.

Despite the high hopes that are connected to these algorithms a true proof or demonstration of any practical

advantage coming from applying a VQA like the QAOA to any real world problem is however still outstanding. Respecting the limitations of existing technology, we neither have large fault tolerant quantum computers nor can we simulate many qubits, a lot of research focus was put on implementations with few qubits and shallow quantum circuits<sup>4,5</sup> and therefore basically ‘proofs of concept’.

In this regime the hopes that are especially put into QAOA seem to face substantial obstacles: already in [2] it was numerically shown, that the MAXCUT problem for 3-regular graphs is not (reliable) solvable with low-depth circuits. Low-depth case studies are done in a broad way through the literature leading to the, at least empirical, conclusion that low depth QAOA circuits will not give reliable results for complicated problem instances<sup>6</sup>.

In this work we extend the investigation of the potential perspectives and limitations of the QAOA to the regime of deep quantum circuits. Central questions that guide us on this path are: What are distinctive features of this regime? Are there effects and methods that become present for deep circuits that are not possible in a low-depth regime? -*And most importantly*- On what classes of problems could QAOA perform well when circuits depth are not a hard limitation?

By this work we try to provide at least some clear answers to those questions. These answers should be, whenever possible, admit a certain aspiration of mathematical rigour and will be backed up by clear intuitions of possible mechanisms and numerical case study evidence otherwise. For a bigger picture we can however only make a beginning.

A distinctive feature for the deep circuit regime concerns the types of classical variational methods that could

<sup>a)</sup>Electronic mail: [kossmann@stud.uni-hannover.de](mailto:kossmann@stud.uni-hannover.de)

<sup>b)</sup>Electronic mail: [binkowski@stud.uni-hannover.de](mailto:binkowski@stud.uni-hannover.de)

<sup>c)</sup>Electronic mail: [timo.ziegler@itp.uni-hannover.de](mailto:timo.ziegler@itp.uni-hannover.de)

<sup>d)</sup>Electronic mail: [rene.schwonnek@itp.uni-hannover.de](mailto:rene.schwonnek@itp.uni-hannover.de)

be employed. In the deep circuit regime we are confronted with a rapidly growing range of classical control parameters. Here the classical variation routines that are typically employed in low-depth QAOA quickly run out of their efficiency range. Instead, we will consider local search routines as the characteristic class of variation methods of the deep circuit regime, since they are naturally suited for optimizations in this situation.

In the first part of [Section III](#), we give a clarified view on the QAOA optimization landscape on state space that is, to our surprise, unexpectedly seldom employed. It however fits well for analyzing local search routines which notably do not admit for a fixed circuit length. The basic QAOA Hamiltonians are treated as generators of a Lie algebra whereby the optimization landscape is given by an orbit of its Lie Group. The resulting landscape reveals a nice geometry that can be analyzed by basic tools from differential geometry. In contrast to the QAOA context, this view is well investigated in the field of optimal control theory from which we borrow methods and results.

In the second part of [Section III](#), we start our investigations by studying the limit of asymptotic circuits. Here we find that a generic QAOA instance has many favourable properties, like a unique local minimum that gives us the optimal solution of the underlying classical optimization problem. This vaguely means that a local search that could exploit arbitrary circuit depths and employ second order gradient methods will succeed in solving almost any problem. This result can be seen in line with findings that were, e.g., reported in [\[7\]](#) showing that variational quantum algorithms with an exponential amount of control parameters can avoid local traps.

These regimes are however far from any practical use. In [Section IV](#) we turn our attention to deep, but not asymptotically deep, circuits. Here many of the nice asymptotic properties vanish. Saddle points turn into effective local minima, and we get a landscape with a continuum of local attractors and potentially exponentially many local traps.

This is however not necessarily the end of all hopes that could be put into QAOA. A characterization of local traps reveals that statistical distribution properties of traps, like amount, sizes, and depths, can be easily accessed by solely evaluating properties of the classical objective function. As a result we introduce performance indicators that allow us to assess if a particular combinatorial optimization problem admits a landscape that is favourable for deep circuit QAOA.

Our method gives strongly problem-dependent quantities that serve as an evaluation basis for the success of the QAOA. Especially the lack of success in many QAOA instances could be explained from this perspective. As an example for a no free lunch behaviour we come up with, in a very simple way, randomly generated target functions that impose an optimization landscape with unfavourably distributed traps. On the other side we however see that certain special problem classes, like QUBO, have the tendency to admit a favourable land-

scape. In [Section V](#) we look at our results from a practical perspective by numerically simulating deep-circuit QAOA based on a very simple downhill simplex method. Results indicate the QAOA performs well only on some classes of optimization problems.

## II. PRELIMINARIES

For the readers convenience we will start by a brief review of the VQA approach, elaborate on the specific form of the QAOA, and outline our view on optimization landscapes, which we will use throughout this work.

### 1. Variational Quantum Algorithms

Consider a generic unconstrained combinatorial minimization problem:

$$\min_{\mathbf{z} \in \mathbb{B}^N} f(\mathbf{z}), \quad (1)$$

where  $\mathbb{B}^N := \{0, 1\}^N$  denotes the set of bit strings of length  $N$ . We follow the standard encoding procedure: identify each bit string  $\mathbf{z}$  with a computational basis state  $|\mathbf{z}\rangle$  of the  $N$ -qubit space  $\mathcal{H} := \mathbb{C}^{2^N}$  and translate the objective function  $f$  into an objective Hamiltonian, diagonal in the computational basis

$$f \mapsto H := \sum_{\mathbf{z} \in \mathbb{B}^N} f(\mathbf{z}) |\mathbf{z}\rangle\langle\mathbf{z}|. \quad (2)$$

Despite mainly working with pure states, we will advocate to describe the state of a quantum system within the formalism of density matrices, i.e. positive matrices  $\rho \geq 0$  of unit trace. We denote the state space by  $\mathfrak{S}(\mathcal{H})$ . An immediate consequence of using this natural formalism is that the expectation value of an observable  $H$

$$F(\rho) := \text{tr}(\rho H) \quad (3)$$

defines a linear functional  $F : \mathfrak{S}(\mathcal{H}) \rightarrow \mathbb{R}$ . Note that by the Rayleigh-Ritz principle, the original minimization task (1) is equivalent to finding a minimum of  $F$ . For our study of derivatives, critical points, and minima of  $F$ , this linearity will turn out as very beneficial.

In order to approximately minimize  $F$ , a general VQA now utilizes parameterized trial states obtained by applying a parameterized quantum circuit to an initial state. For the QAOA, the initial state is given by the pure state  $|+\rangle\langle+|$ , where

$$|+\rangle = \bigotimes_{n=1}^N \frac{1}{\sqrt{2}} (|0\rangle + |1\rangle) = \frac{1}{\sqrt{2^N}} \sum_{\mathbf{z} \in \mathbb{B}^N} |\mathbf{z}\rangle. \quad (4)$$

It is the non-degenerate ground state of the Hamiltonian<sup>8</sup>

$$B = - \sum_{n=1}^N \sigma_x^{(n)}. \quad (5)$$

The unitary evolution generated from  $B$  is commonly referred to as 'mixing'.

For QAOA we have two basic families of gates

$$U_B(\beta) = e^{-i\beta B} \quad \text{and} \quad (6a)$$

$$U_C(\gamma) = e^{-i\gamma C}, \quad (6b)$$

where we used the convention of taking  $C = H - \text{tr}(H)\mathbb{1}$  as a traceless generator for our second unitary, which is usually coined the 'phase separator'. Note that taking all generators traceless does not change the evolution on the level of density matrices.

A full QAOA circuit is then combined from these basic families. The corresponding parameters are typically labeled by  $\vec{\beta} = (\beta_1, \dots, \beta_p) \in [0, \pi]^p$  and  $\vec{\gamma} = (\gamma_1, \dots, \gamma_p) \in \mathbb{R}^p$  with  $p \in \mathbb{N}$ , where the quantity  $p$  specifies the circuit depth. A fully parameterized QAOA circuit is therefore given by

$$V(\vec{\beta}, \vec{\gamma}) = \prod_{q=1}^p U_B(\beta_q) U_C(\gamma_q) \quad (7)$$

## 2. The deep circuit regime

In the majority of the existing literature circuits with a depth  $p \approx 10$  or less are taken into account. One practical reason for this restriction is the still too high gate noise in existing quantum computers.

In this work we will refer to deep circuits as those that substantially exceed the scale of  $p \approx 10$ , potentially by orders of magnitudes. For example, the circuit depths used in our numerical simulations ranged from 100 to  $3 \cdot 10^4$ . From a technological perspective, this regime is not yet reliably realizable on most existing devices, but clearly at the edge of what we can expect from the technological developments in the near and midterm future. The key achievements we are here hoping for are improved gate fidelities that could, e.g. be enabled by improved error mitigation techniques<sup>9</sup> or even a full implementation of (few) error corrected qubits<sup>10</sup>.

A central ingredient in any VQA are the classical routines involved in optimizing the circuit parameters. Here the types of classical optimization algorithms that can be used for shallow or deep circuits might differ substantially. In shallow circuits all variational parameters can be actively optimized at the same time. Typical optimizers in use are for example COBYLA, Gradient Descent, and Nelder-Mead. Those may however not perform well for deep circuits. An optimization of a largely growing amount of parameters might quickly become unpractical, either by an increase of computational hardness or by the commonly observed barren plateaus<sup>11,12</sup>.

For deep circuits we will therefore focus on optimization routines that follow local search strategies, i.e. those which successively only vary a few parameters at the same time within a small range of variation. We tend

to mark the necessity of these routines as another distinguishing feature of the deep circuit regime. As a naive prototype, we used a very simple downhill simplex method in our numerical studies in Section V, being fully aware that a huge variety of very elaborated and versatile local search routines exist.

## 3. Optimization Landscapes

In the context of QAOA the term optimization landscape commonly refers to the 'landscape' of values that the functional  $F$  takes on a parameter space that is a subset of  $\mathbb{R}^{2p}$  (or on a two dimensional subspace whenever a graphical illustration is provided).

However, for local search strategies the final length  $p$  of a circuit, and therefore the parameter space, is typically not fixed. Rather than that certain termination criteria like a fixed target precision will be imposed. Hence, the above notion of 'optimization landscape' does not really apply here. This motivates us to think of optimization landscapes in a different way:

We simply regard the functional  $F$  as a function that defines a 'landscape' on the state space  $\mathfrak{S}(\mathcal{H})$ , or more precisely on the subset of the states that are potentially accessible by a sequence of QAOA gates. To our big surprise, this perspective is rather rare to find within the existing literature on VQAs. It's indeed very nice geometry will therefore be fully clarified within the next section.

In order to properly distinguish notions we will from now on refer to landscape in  $\mathbb{R}^{2p}$  as the *parameter landscape* of  $F$  and to the latter one as the *state space landscape* of  $F$ . Using the state space landscape to determine properties of an QAOA algorithm has at least three immediate advantages:

- (i) Circuits with varying length can be properly expressed and compared within the same picture.
- (ii) Local overparameterization is avoided. Different sets of parameters could refer to almost the same point in statespace in no obvious way. This can, for example, lead to a situation in which there are many different local minima in the parameter landscape that however only correspond to one and the same minimum in the statespace landscape.
- (iii) The behaviour of different classes of VQAs can be compared within the same picture.

In this work, especially the points (i) and (ii) will be essential for analyzing the performance perspectives of deep QAOA circuits by characterizing the distribution properties of local minima and critical points.

### III. ASYMPTOTIC CIRCUITS

As starting point of our investigation we will discuss the perspectives of the QAOA in an asymptotic regime. This is, we consider infinite sequences of gates with potentially infinitesimally small parameters. By including infinitesimal elements, the analysis of the asymptotic QAOA becomes drastically more structured since we now can make direct use of tools from differential geometry, i.e. Lie groups and their algebras.

In the first part of this section we will clarify this geometry. Here the key points are:

- Accessible states form a differentiable manifold  $\Omega$
- The target functional corresponds to a differentiable scalar field on  $\Omega$
- The two families of QAOA gates correspond to two vector fields on  $\Omega$

We will then turn our attention to the classification of minima and critical points of  $F$ . Here our key findings for generic instances are:

- We have a one to one correspondence between the possible solution space  $\mathbb{B}^N$  of the classical optimization problems and critical points of  $F$
- Within these critical points there is only one local minimum. This minimum is the solution of the underlying optimization problem.

Thematically, our investigations and results belong to the field of dynamical Lie algebras (see [13] for a comprehensive review). However, we see our analysis as more tangible than the general case discussed there.

#### 1. The geometry of accessible states

The first question that arises when considering asymptotic gate sequences is: which states can be reached by the QAOA when starting from an initial state  $\psi_0$ ? This set, from now on denoted by  $\Omega$ , will be the ground for the geometrical picture we want to outline in this section.

Let  $H$  be the target Hamiltonian that encodes an optimization problem and let  $U_B(\beta)$  and  $U_C(\gamma)$  with  $C = H - \text{tr}(H)\mathbb{1}$  be our basic families of QAOA unitaries as described in the previous section. The set  $\Omega$  will be obtained from considering the set  $G(B, C)$  of all circuits that could be asymptotically generated by the QAOA. In the following, we will drop the explicit dependence on  $B$  and  $C$  and write  $G = G(B, C)$  whenever it is clear from the context.

#### Circuits

As described in the previous section, circuits of a fixed depth  $p$  are parameterized by finite sequences of angles

$\vec{\gamma}$  and  $\vec{\beta}$ . For any  $p$  these can be captured by the set

$$G_p = \left\{ \prod_{i=1}^p U_C(\gamma_i) U_B(\beta_i) \in \text{SU}(2^N) \mid (\vec{\gamma}, \vec{\beta}) \in \mathbb{R}^{2p} \right\}. \quad (8)$$

There are now some technicalities to respect when considering circuits of infinite depth. A naive limit  $p \rightarrow \infty$  of infinite angles sequences in (8) will lead to infinite products of unitaries, which is not necessarily a well-defined object.

However, on the level of sets we observe that the  $G_p$  form a monotone sequence, i.e. we have  $G_p \subseteq G_{p+1}$ . Here a well-defined set-theoretic limit exists. From this limit we obtain  $G$  by taking the topological closure in  $\mathcal{L}(\mathcal{H})$ , i.e. by

$$G = \overline{\left( \lim_{p \rightarrow \infty} G_p \right)} \subset \text{SU}(2^N). \quad (9)$$

Intuitively,  $G$  contains all circuits of finite depth such as all unitary transformations that can be approximated by them up to arbitrary precision. Here proximity is measured in the operator norm, meaning that two unitaries will be close to each other whenever their images are close to each other for any input state.

#### States

Applying these circuits to a fixed initial state  $\Psi_0$ , i.e. taking the  $G$ -orbit around  $\Psi_0$ , will then give us the set  $\Omega$  of accessible states

$$\Omega := \{U\Psi_0U^* : U \in G\} \subseteq \mathfrak{S}(\mathcal{H}). \quad (10)$$

Corresponding to our intuition on  $G$ , those are all states that can be generated from  $\Psi_0$  by a finite circuit such as all states that are approximately close to them. The central observation for the following analyses is that the set  $G$  naturally carries the structure of a Lie group, which will also carry over to a corresponding structure on  $\Omega$ .

On one hand, a Lie group has the structure of a group, which in this case simply reflects that QAOA circuits have some of the basic properties a complete set of quantum circuits should have. The group action, here given by multiplying the corresponding unitaries, reflects that concatenating two possible circuits gives again a valid circuit. The existence of a neutral element, the identity operator, is obtained by setting all angles  $\vec{\gamma}$  and  $\vec{\beta}$  to zero. This corresponds to an empty circuit, i.e. doing nothing. The existence of an inverse<sup>14</sup>, here provided by taking the adjoint of a unitary, reflects the often advertised property that quantum circuits are reversible and that the set of QAOA circuits is complete with respect to this property.

On the other hand, the Lie group  $G$  has the structure of a manifold. This structure will be crucial for rigorously talking about optimization landscapes in what follows. Even though the manifold structure of a Lie group is



given in a quite abstract manner in the first place<sup>15</sup>, it will carry over to a concrete structure on  $\Omega$ , giving us the playground for defining optimization landscapes and analyzing the behaviour of optimization routines.

For  $\omega \in \Omega$  and  $U \in G$  the map

$$\pi_\omega(U) := U\omega U^* \quad (11)$$

describes an action of  $G$  on  $\Omega$  and defines the Lie group structure on  $\Omega$ . Firstly,

$$\pi_{\pi_\omega(V)}(U) = UV\omega V^*U^* = \pi_\omega(UV) \quad (12)$$

gives us a group homomorphism. Secondly, as outlined later on, this map will also carry over the manifold structure from  $G$  to  $\Omega$ . As a manifold,  $\Omega$  is isomorphic to the Lie group quotient  $G/N$  via the map  $\pi_{\Psi_0}$  where  $N = \{U \in G : U\Psi_0U^* = \Psi_0\}$ . A direct consequence is that  $\Omega$  is a closed manifold, i.e. is compact and has no boundary.

### The objective

Our target functional  $F(\omega) = \langle H \rangle_\omega$  can now be seen as a scalar field  $F : \Omega \rightarrow \mathbb{R}$ . Our initial minimization task is hence equivalent to finding the minimum of this field on  $\Omega$ . A direct consequence that can be drawn from the fact  $\Omega$  is a closed manifold is that local and global minima only occur in the interior. It is easy to see that  $F$  is indeed also differentiable, which directly implies that local minima can be characterized considering its derivatives.

Derivatives on a manifold are given in terms of tangent spaces. The tangent spaces on  $G$  are obtained from its Lie algebra. We will denote the Lie algebra that corresponds to  $G$  by  $\mathfrak{g}(B, C)$ . It always contains the Lie algebra generated by  $iB$  and  $iC$ :

$$\begin{aligned} \mathfrak{g}(B, C) &\supseteq \text{Lie}(\{iB, iC\}, [\cdot, \cdot]) \\ &= \text{span}_{\mathbb{R}} \{iB, iC, [B, C], i[B, [B, C]], \dots\}. \end{aligned} \quad (13)$$

The question of equality in (13) is subtle, but not too important for our analysis. We will drop the explicit dependence on  $B$  and  $C$  in the notation and write  $\mathfrak{g} = \mathfrak{g}(B, C)$  whenever it is clear from the context. Our choice of taking  $B$  and  $C$  to be trace-less implies that  $\mathfrak{g} \subseteq \mathfrak{su}(\mathcal{H})$ . The map  $\pi_\omega$  now transfers the tangent spaces of  $G$  to tangent spaces on  $\Omega$ . More precisely, for a point  $\omega \in \Omega$  the map  $\pi_\omega$  gives us a push forward from  $\mathfrak{g}$  to the tangent space  $T_\omega\Omega$  at  $\omega$ .

Resulting from this we can introduce the directional derivatives of a scalar field w.r.t.  $A \in \mathfrak{g}$  at a point  $\omega \in \Omega$  by

$$\begin{aligned} \nabla_A^{(n)} F(\omega) &:= \partial_t^{(n)} F(\pi_\omega(e^{tA}))|_{t=0} \\ &= \partial_t^{(n)} F(e^{tA} \omega e^{-tA})|_{t=0}. \end{aligned} \quad (14)$$

These derivatives will be used to characterize critical points, minima, and maxima in the subsequent sections. At each point  $\omega \in \Omega$ , there will be several  $A \in \mathfrak{g}$  that

do not correspond to actual directions on  $\Omega$  due to its quotient structure. Namely, for  $A \in \mathfrak{g}$  with

$$[\omega, A] = 0, \quad (15)$$

we have that  $\pi_\omega(e^{tA}) \equiv \omega$  for all  $t \in \mathbb{R}$ . Thus, the directional derivatives w.r.t.  $A$  would vanish for every considered scalar field and is therefore meaningless.

### QAOA sequences

To complete this section we will have a look at the geometric role that the families of basic QAOA gates  $U_B(\beta)$  and  $U_C(\gamma)$  play. From the manifold perspective those correspond to vector fields  $\Phi_B$  and  $\Phi_C$  on  $\Omega$ . Explicitly, we can think of vectors

$$i[\omega, B] \text{ and } i[\omega, C] \quad (16)$$

that are assigned to each point  $\omega \in \Omega$ . The structure of these vectors can be grasped in a simple manner by considering that a point  $\omega$  is transported by a one parameter family  $U_t = e^{tA}$  via the map (11) along a continuous curve  $\omega_t = \pi_\omega(e^{tA})$  on  $\Omega$ . The directional derivative along this curve is then simply given by

$$\partial_t \omega_t|_{t=0} = \partial_t e^{tA} \omega e^{-tA}|_{t=0} = -[\omega, A]. \quad (17)$$

Performing a QAOA instance of depth  $p$  with some parameters  $\beta_1, \beta_2, \dots, \beta_p$  and  $\gamma_1, \gamma_2, \dots, \gamma_p$  hence can be understood in a nice geometrical picture: start from  $\Psi_0$  and follow (the flow of) the vector field  $\Phi_C$  for a distance given by parameter  $\gamma_1$ , stop and change direction to follow the (flow of the) vector field  $\Phi_B$  for a distance given by  $\beta_1$ , and so on. Here the circuit depth  $p$  determines the number of switching from one flow to the other. Situations in which shallow circuits suffice to reach a global minimum can therefore be associated to situations in which the vector fields have a simple structure (see for example Figure 1). In converse, we expect that the, potentially exponential, hardness of a particular classical problem translates into a corresponding complexity of the vector field structure. Here the dimension of the corresponding Lie algebra would be a natural number for quantifying this.

## 2. The Lie algebra of the encoded problem

For the characterization of optimization landscapes we will first focus on the underlying manifold. Here, the central question is: which Lie group corresponds to a classical optimization problem encoded in a given Hamiltonian  $H$ ? As the shape of a Lie group is fully encoded in its Lie algebra it already suffices to focus on this object. Here the above question translates to determining properties of the algebra  $\mathfrak{g}$  which is generated by given operators  $B$  and  $C$ .

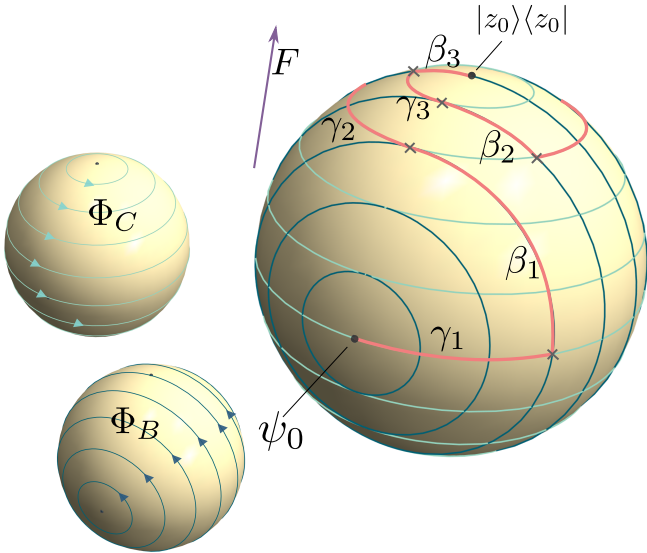


FIG. 1: The geometry of the QAOA visualized on a qubit: here  $\Omega$  is given by the surface of the Bloch sphere (all pure qubit states). Applying the basic gates  $U_C$  or  $U_B$  corresponds to moves along vector fields  $\Phi_C$  or  $\Phi_B$  that are oriented along lines of constant latitudes (left). Performing a QAOA sequence (coral colored line) corresponds to alternatingly move along these vector fields.

The precise form of  $\mathfrak{g}$  might however be highly problem specific and will reflect the hardness of the underlying classical optimization problem becomes, in general, extremely hard to compute for large systems.

At this point, we will leave the detailed investigation of this connection for future work and instead provide statements on  $\mathfrak{g}$  for a generic case.

Notably, it was prominently shown<sup>16,17</sup> that almost every set of quantum logic gates with an action on more than one qubit can be used to generate any quantum circuit. A corresponding result for Lie algebras states that the algebra generated by randomly drawn traceless matrices almost certainly turns out to be the full algebra  $\mathfrak{su}(2^N)$ . This clearly suggests to ask for a similar behaviour in the special case of the QAOA circuits.

Formally, we will say that the generators  $B$  and  $C$  of QAOA-gates are *universal* if  $G(B, C) = \text{SU}(\mathcal{H})$ . This follows automatically if the Lie algebra generated by  $iB$  and  $iC$  is  $\mathfrak{su}(\mathcal{H})$ . Clearly, this question has been investigated before<sup>18</sup> with the result that universality of QAOA circuits was proven for a wide range of objective Hamiltonians  $H$  and their corresponding generator  $C$ . The following theorem will contribute to this by a simple sufficient criterion for universality that can easily be checked by merely considering the possible values of the classical objective function  $f$ . In the field of optimal control theory the notion of ‘controllability’ is the counterpart to the universality of a gate set in our case. Based on a convenient controllability criterion from [19] we get

**Theorem 1.**  $B$  and  $C$  form universal generators of QAOA-gates if the underlying classical optimization problem given by a target function  $f$  fulfills the conditions

(a) non-degenerate values:

$$f(z) = f(z') \implies z = z'$$

(b) non-degenerate resonance:

$$f(z) - f(z') = f(t) - f(t') \implies (z, z') = (t, t')$$

if  $z \neq z'$  and  $t \neq t'$ ,

In particular, the set of optimization problems  $f$ , for which  $\mathfrak{g} = \mathfrak{su}(2^N)$ , is open and dense (and hence the complement is a null set).

The proof of this theorem can be found in the Appendix. If one has  $\mathfrak{g} = \mathfrak{su}(2^N)$ , then it is always possible to solve the problem in finitely many steps, i.e., there exist  $\beta_j, \gamma_j$ ,  $j = 1, \dots, k$  such that  $U_B(\beta_1)U_C(\gamma_1)U_B(\beta_2) \cdots U_C(\gamma_k)$  maps the initial state to a ground state of  $H$  (see [20, Thm. 3.4]).

Thus, a randomly chosen optimization target  $f$  will fulfill the criteria from Theorem 1 almost certainly, in which case we call  $f$  *severing*. We can therefore draw the conclusion that universality is indeed a generic property of the QAOA. Generic instances of Knapsack, where the values and weights are arbitrary real numbers, or Traveling Salesman, where the distances between cities are arbitrary real numbers, (both encoded with soft constraints) will fall in this category. Furthermore, generic QUBOs are one of the classes for which universality was shown in [18].

Problem classes where values of  $f$  are typically given by integers, like MAXCUT or MAX- $k$ -SAT, do however not necessarily fulfill the conditions of Theorem 1 and could therefore lead to an optimization on smaller sets. If universality is a desired property, it can however always be restored by adding small perturbation. A concrete strategy would be to consider weighted MAXCUT or weighted MAX- $k$ -SAT, with close to integer weights. The universality in these cases is ensured by the denseness statement in Theorem 1.

In general, it is however far from obvious whether a lack of universality is an obstacle or an actual feature. On one hand, we have that the reachable set  $\Omega$  becomes  $\mathcal{P}(\mathcal{H})$ , the whole set of pure states when  $\mathfrak{g} = \mathfrak{su}(2^N)$  and thus, the largest possible search space. A smaller algebra would in turn lead to a smaller search space, which may make finding an optimum an easier task. However, on the other hand, a bigger algebra in principle also gives more paths that could be taken by the QAOA, which may in contrast enhance our chances to find short paths, which is one of the QAOA’s advertised features. Another feature of universality that we will explore in the following is that a sufficiently big algebra will prohibit the existence of local minima in the optimization landscapes. Here the

intuition would be that a larger algebra provides us with more directions to move towards in order to escape from local extrema.

### 3. Classification of critical points

With the basic geometry set up in the previous subsections we can now turn our attention to our intended task of minimizing a target functional  $F$ . As mentioned above, it is clear from the underlying manifold structure that the global minimum of  $F$  on  $\Omega$ , the point we want to find, does not occur on any boundary. Hence, we will now follow the usual procedures for discussing the extreme points of a differentiable function. We start by considering critical points:

We call  $\omega_0 \in \Omega$  a *critical point* of  $F$  provided that  $\nabla_A F(\omega_0)$  vanishes for all  $A \in \mathfrak{g}$ . It is clear that any minimum has to be within the set of critical points. Furthermore, the existence of critical points also plays a major role for the deep QAOA based on local optimization strategies. Here critical points typically appear as local attractors, which may impose major hurdles for a good overall performance. In the universal case, the critical points can be identified as the eigenstates of  $H$ .

**Proposition 2.** *Let  $B$  and  $C$  be universal generators of QAOA-gates. Then the critical points of  $F$  are precisely the eigenstates of  $H$ .*

*Proof.* For an arbitrary  $\omega \in \Omega$  and  $A \in \mathfrak{g}(B, C)$  it holds that

$$\begin{aligned} \nabla_A F(\omega) &= \partial_t \operatorname{tr} (H e^{tA} \omega e^{-tA}) |_{t=0} \\ &= \operatorname{tr}(HA\omega) - \operatorname{tr}(H\omega A) \\ &= \operatorname{tr}(A\omega H) - \operatorname{tr}(AH\omega) \\ &= \operatorname{tr}(A[\omega, H]). \end{aligned} \quad (18)$$

Now  $\omega$  is an eigenstate of  $H$  if and only if the commutator  $[\omega, H]$  vanishes. Thus, all eigenstates of  $H$  that lie in  $\Omega$  are critical points. However, since we assume  $B$  and  $C$  to be universal,  $\Omega = \mathcal{P}(\mathcal{H})$  holds. Conversely, let  $\operatorname{tr}(A[\omega, H]) = \operatorname{tr}(\omega[A, H])$  vanish for all  $A \in \mathfrak{g}(B, C)$ . Due to the assumed universality of  $B$  and  $C$ , we can choose  $A = [\omega, H]^*$  and conclude that  $\|[\omega, H]\| = 0$ . Therefore,  $\omega$  is already an eigenstate of  $H$ .  $\square$

If the classical target function  $f$  is severing, all eigenstates of  $H$  are non-degenerate and therefore coincide with the computational basis states. Thus, we conclude

**Corollary 3.** *Let  $f$  be severing. Then the critical points of  $F$  are precisely the computational basis states.*

The last proposition tells us, that the state we are looking for is a critical point of the functional. Moreover, there are no irregularities in terms of ‘hidden’ minima for some special functional.

### 4. Uniqueness of minima and maxima

Next, we want to go one step further and investigate properties of the second derivatives. These will allow us to distinguish between local minima, maxima, and saddle points. In fact, we have the following necessary condition for local extrema.

**Corollary 4.** *If  $\omega_0 \in \Omega$  is a local minimizer of  $F$  then  $\omega_0$  is a critical point of  $F$  and for all  $A \in \mathfrak{g}$  it holds that  $\nabla_A^{(2)} F(\omega_0) \geq 0$ .*

Any critical point of  $F$  with indefinite second derivatives we call *saddle point*. In the universal case, the critical points of  $F$  are precisely given by the eigenstates of  $H$  due to [Proposition 2](#). This allows us to classify the local minima even further. Namely, local minima are already global ones.

**Proposition 5.** *Let  $B$  and  $C$  be universal generators of QAOA-gates. Then each local minimum of  $F$  is already its global minimum and corresponds to a ground state of  $H$ .*

*Proof.* By the Rayleigh-Ritz inequality, all global minima of  $F$  correspond to ground states of  $H$ . Let  $\lambda_0$  denote its ground state energy. Now, let  $|\psi\rangle\langle\psi| \in \Omega$  be a local minimizer of  $F$ . By [Proposition 2](#) and [Corollary 4](#),  $|\psi\rangle\langle\psi|$  is an eigenstate of  $H$ ; let  $\lambda$  denote the corresponding eigenvalue. Furthermore, for all  $A \in \mathfrak{g}(B, C)$  it holds that

$$\begin{aligned} 0 \leq \nabla_A^{(2)} F(|\psi\rangle\langle\psi|) &= \partial_t^2 \operatorname{tr} (e^{tA} |\psi\rangle\langle\psi| e^{-tA} H) |_{t=0} \\ &= 2 \operatorname{tr} (|\psi\rangle\langle\psi| (A^2 H - A H A)) \\ &= 2 \operatorname{tr} (A |\psi\rangle\langle\psi| A (\lambda \mathbb{1} - H)) \\ &= 2 \operatorname{tr} (A |\psi\rangle\langle\psi| A^* (H - \lambda \mathbb{1})) \\ &= 2 (\langle A\psi | H | A\psi \rangle - \lambda \langle A\psi | A\psi \rangle) \end{aligned} \quad (19)$$

If  $|\psi\rangle\langle\psi|$  would not be a ground state of  $H$ , one could choose  $A \in \mathfrak{g}(B, C) = \mathfrak{su}(2^N)$  so that  $A |\psi\rangle\langle\psi| A^*$  is an (unnormalized) ground state of  $H$ , implying that  $\lambda_0 \geq \lambda$  which clearly rises a contradiction.  $\square$

If the classical target function  $f$  is severing, the degeneracy of the global minima is lifted and we obtain

**Corollary 6.** *Let  $f$  be severing. Then  $F$  admits its only local and global minimum at  $|\mathbf{z}_0\rangle\langle\mathbf{z}_0|$ , where*

$$\mathbf{z}_0 = \arg \min_{\mathbf{z} \in \mathbb{B}^N} f(\mathbf{z}).$$

In summary, a generic classical optimization problem, that is, with severing objective function  $f$ , induces a very simple optimization geometry on  $\Omega$ : the critical points of  $F$  precisely are the computational basis states and the only local and also global minimum is obtained at the state corresponding to the optimal solution to  $f$ . Conversely, at any other point  $\omega \in \Omega$ , we can always find

a direction  $A \in \mathfrak{g}$  along which the functional  $F$  strictly decreases. This simple structure is partially lost in the following chapter, where we only allow certain directions. The loss of information results in the appearance of additional local minima.

Our previous results are to be compared with [7]: While we show the absence of local minima in the state space landscape, they prove that certain VQA ansätze for MAXCUT result in local minimum-free parameter landscapes.

#### IV. DEEP CIRCUITS

We will now discuss the regime of deep circuits. Here we consider local search routines on circuits with large but not fixed  $p$ . For this we can keep in mind an intuitive picture of what a local search does: in search of the minimum of  $F$ , we maneuver through the state space landscape by small steps. In doing so, we are limited to only evaluate  $F$  point-wisely and locally.

In contrast to the asymptotic regime from the previous section, we no longer assume that we can move in any direction from  $\mathfrak{g}$ . In the explicit case of the QAOA the remaining directions are  $iB$  and  $iC$ , since moving in any another direction, like for example  $[B, C]$ , would in principle require an infinite sequence of infinitesimal gates.

Additionally, it is not guaranteed that all states from  $\Omega$  can be reached by circuits with a depth  $p$  of reasonable order of magnitude.

##### 1. Local Attractors and Traps

As a direct consequence of restricting search movements to the directions  $iB$  and  $iC$ , it can happen that we lose the ability of escaping from a saddle point. By this we effectively get new additional local minima when transiting from the asymptotic to the deep circuit regime. As we will see, those can in fact be uncountable many.

As before we can identify local minima by looking at first and second derivatives in the available movement directions. Since  $F$  stays constant under transformations in  $iC$  direction, we only have to consider directional derivatives in the direction  $iB$ . At a state  $\phi$  those are given by

$$\nabla_B^{(1)} F(\phi) = i \operatorname{tr}(\phi [B, H]) =: \operatorname{tr}(\phi F_1^B) \quad (20)$$

and

$$\nabla_B^{(2)} F(\phi) = -2 \operatorname{tr}(\phi [B, [B, H]]) =: \operatorname{tr}(\phi F_2^B). \quad (21)$$

We substitute operators  $F_1^B$  and  $F_2^B$ , as above, to shorten notations in the following. A state will turn into a local

minimum for deep circuits if the second derivative is positive and the first derivative vanishes. This corresponds to a semi-definitely constrained set

$$\mathcal{T}_B := \{\phi \in \Omega \mid \operatorname{tr}(\phi F_1^B) = 0 \text{ and } \operatorname{tr}(\phi F_2^B) > 0\}. \quad (22)$$

Such a set will typically contain a full continuum of points. To get an intuition for this we can embed  $\Omega$  into the Hilbert-Schmidt space. Here fulfilling the conditions for membership in (22) corresponds to the intersection of the state space with a high dimensional half space and a high dimensional subspace. Note that, in the generic case  $\mathcal{T}_B$  will be disjoint. In the following, we will refer to its conjoint components as *troughs*.

Our findings suggest that troughs are attracting regions for the QAOA with local search routines.

On an empirical level, we observe this behaviour throughout our numerical studies. More details are given in Section V. On a theoretical level, a fully rigorous proof for this is unfortunately difficult to provide, since the full body of local search routines is hard to capture in a mathematical statement. We can however give some clear theoretical intuitions: By construction we have that, when starting from an arbitrary state  $\phi$ , the minimization of  $F$  along a trajectory  $\pi_\phi(e^{i\beta B})$ , this is, only moving along direction  $iB$ , will end up in  $\mathcal{T}_B$ . For a very simple local search routine, this is indeed likely to happen, since following this direction will guarantee a monotonous descent. Performing  $iC$  movements in between might prevent this behaviour. In this case the search routine may follow a more complicated path. If, at the end, this routine however also minimizes gradients in the  $\beta\gamma$  parameter landscape it will end up in  $\mathcal{T}_B$ , as well.

Once a search routine comes close to a trough a local search can not leave the environment of a trough besides performing global movements (we will call them jumps). The behaviour in such a situation is a forward and backward bouncing along the 'walls' of the trough. This behaviour is typical for local search routines and we also observe it throughout our numerical studies (see e.g. Figure 12).

In the case of the QAOA an intuitive explanation for this can be given. Moving away from a trough by an  $iB$  movement will increase the value of  $F$  and will hence be suppressed by a routine that looks for local optimality. We will therefore run into a circle in which movements into  $iC$  direction, which leave the value of  $F$  invariant, are followed by a step in  $iB$  direction which moves back towards the trough. An usual problem in such situation is that, even though many steps are performed, the value of the functional will not, or only very slowly, improve. Even though, refined routines like the conjugate gradient method<sup>21</sup>, tend to avoid this behaviour and adapting them for our special situation in the QAOA seems plausible, there are points within a trough where local search routines have to face further obstacles.

We recall from Section III that all non-optimal eigenstates of  $H$  correspond to saddle points in the landscape. Here first derivatives vanish, such that those states are



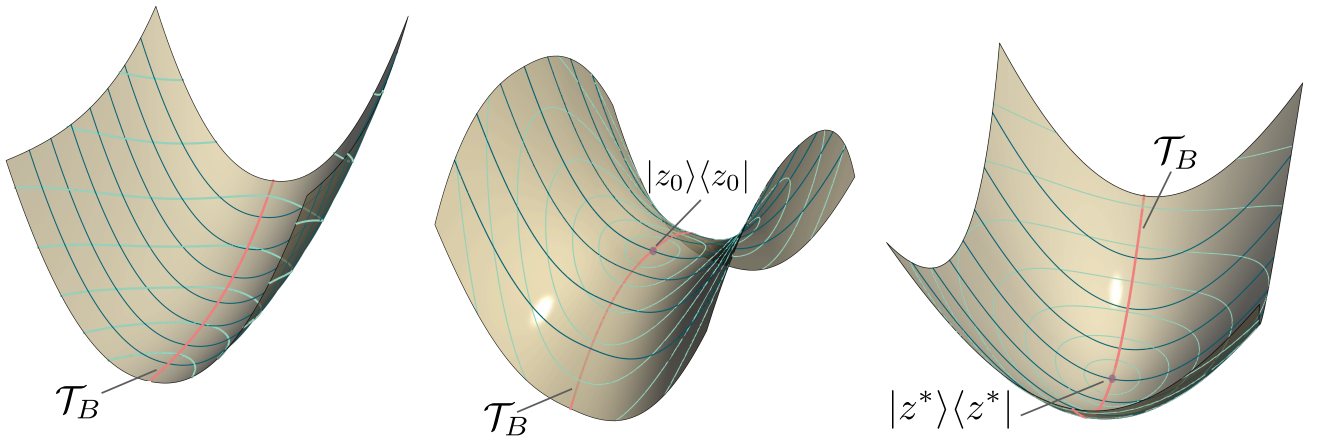


FIG. 2: Schematic visualization of different troughs without any computational state, including a local extremum  $|z_0\rangle\langle z_0|$ , and the optimal state  $|z^*\rangle\langle z^*|$ , respectively.

located in  $\mathcal{T}_B$  whenever their second derivative into  $iB$  direction is positive. Eigenstates of  $H$  are also eigenstates of  $C$  and by this have the property that they are invariant under  $iC$  movements. Additionally we also have that any point close to them will stay close under  $iC$  movements. We can see this by checking that the trace distance (which is unitarily invariant) between a state  $\phi$  and an eigenstate  $|z_0\rangle\langle z_0|$  stays constant along a  $iC$  trajectory, i.e. we have

$$\begin{aligned} \|\pi_\phi(e^{i\gamma C}) - |z_0\rangle\langle z_0|\|_1 &= \|e^{-i\gamma C} \phi e^{i\gamma C} - |z_0\rangle\langle z_0|\|_1 \\ &= \|\phi - e^{-i\gamma C} |z_0\rangle\langle z_0| e^{i\gamma C}\|_1 \\ &= \|\phi - |z_0\rangle\langle z_0|\|_1. \end{aligned} \quad (23)$$

As a result we observe that a local search around the  $H$  eigenstates that are in  $\mathcal{T}_B$  will tend to get stuck. Due to the saddle point property, the functional will be almost constant, and no  $iC$  step allows to leave the region. We will mark those points as *traps*.

Let  $|z_0\rangle\langle z_0|$  be an eigenstate of  $H$  with eigenvalue  $f(z_0)$ . In order to decide if this state is in  $\mathcal{T}_B$  we have a look at its second derivative in  $iB$  direction. Using the computation in (19) we get

$$\begin{aligned} \nabla_B^{(2)} F(|z_0\rangle\langle z_0|) &= \text{tr}(|z_0\rangle\langle z_0| F_2^B) \\ &= 2 \left( \sum_{\Delta(z_0, z)=1} f(z) - N f(z_0) \right), \end{aligned} \quad (24)$$

where  $\Delta(z, z')$  denotes the Hamming distance between the two bit strings  $z$  and  $z'$ . This expression has a nice interpretation. In the above, the sum

$$\sum_{\Delta(z_0, z)=1} f(z) = \langle z_0| B^2 |z_0\rangle$$

comes from the special form of  $B$  that is characteristic for the QAOA. Up to a factor  $N$ , it can be interpreted as the average of  $f$  taken over all next nearest neighbors of  $z_0$  in the hypercube  $\mathbb{B}^N$ . For what follows, it is useful to define the quantity

$$\mu(z_0) := \sum_{\Delta(z_0, z)=1} \frac{f(z) - f(z_0)}{N}, \quad (25)$$

which can be understood as the average difference between the value of  $f$  on  $z_0$  and all neighboring strings. This average is proportional to the second derivative and suffices to determine what happens to the saddle point at  $z_0$  when restricting to the deep circuit regime.

Moreover, note that a string  $z_0$  of length  $N$  has only  $N$  neighbours in  $\mathbb{B}^N$ . Therefore, the quantity  $\mu(z_0)$  can be efficiently determined by a classical computation that merely has to check and add the values of  $f$  at those points.

## 2. Trap sizes

Once a local search is stuck in a trap, jumps, i.e. steps on a larger scale, have to be performed in order to escape. We can give an estimate on the required jump size by considering the distance from a trap to the closed state with negative second derivative. This, arguably heuristic, quantity will give us the scale on which the local behaviour around a trap stops to dominate. See Figure 3 for a visualization. From now on, we will refer to a region around a trap in which all second derivatives are non-negative as *valley*.

Assume a trap centred at a state  $|z_0\rangle\langle z_0|$  and an  $\varepsilon$ -neighbourhood

$$\{\rho_\varepsilon \in \Omega : \|\rho_\varepsilon - |z_0\rangle\langle z_0|\|_1 < \varepsilon\}.$$

By definition we can express any state in this neighborhood as

$$\rho_\varepsilon = |\mathbf{z}_0\rangle\langle\mathbf{z}_0| + \varepsilon K \text{ with } \|K\|_1 \leq 1,$$

and we can bound the second derivative of  $\rho_\varepsilon$  by the estimate

$$\begin{aligned} \nabla_B^{(2)} F(\rho_\varepsilon) &= \text{tr}(\rho_\varepsilon F_2^B) \\ &\geq \inf_{\|K\|_1 \leq 1} (\text{tr}(|\mathbf{z}_0\rangle\langle\mathbf{z}_0| F_2^B) + \varepsilon \text{tr}(K F_2^B)) \\ &= 2N\mu(\mathbf{z}_0) - \varepsilon \sup_{\|K\|_1 \leq 1} \text{tr}(K F_2^B) \\ &= 2N\mu(\mathbf{z}_0) - \varepsilon \|F_2^B\|_\infty \end{aligned} \quad (26)$$

where we used Hölder's inequality in the last step. Thus, by computing or estimating the universal factor  $\|F_2^B\|_\infty$  for an explicit problem instance, one can estimate the size of a valley in the state space landscape by asking for all  $\varepsilon$ -neighbourhoods in which all second derivatives are positive. From the last line of (26) we get a bound

$$\varepsilon < \frac{2N\mu(\mathbf{z}_0)}{\|F_2^B\|_\infty} \quad (27)$$

on the critical  $\varepsilon$ .

Moreover, we can give an upper bound on  $\|F_2^B\|_\infty$  by exploiting the sub-multiplicativity of the operator norm and get

$$\begin{aligned} \|F_2^B\|_\infty &= \|[B, [B, C]]\|_\infty \\ &\leq 4\|B\|_\infty^2 \|C\|_\infty = 4N^2 \|C\|_\infty. \end{aligned} \quad (28)$$

In combination with (27) we can conclude

$$\varepsilon < \frac{\mu(\mathbf{z}_0)}{2N\|C\|_\infty}. \quad (29)$$

This estimate has the natural interpretation, that the region around an eigenstate, especially around the global minimum, where one observes the properties of the  $B$  derivative at this eigenstate gets smaller with growing problem size ( $\sim \frac{1}{N}$ ). Furthermore we can include the operator norm of  $C$  into  $\mu$ , by observing that in  $\mu$  we can always consider normalized eigenvalues (w.r.t. the biggest one). This yields a redefinition

$$\tilde{\mu}(\mathbf{z}_0) := \sum_{\Delta(\mathbf{z}_0, \mathbf{z})=1} \frac{C(\mathbf{z}) - C(\mathbf{z}_0)}{N \cdot \|C\|_\infty} \quad (30)$$

such that

$$\varepsilon \leq \frac{\tilde{\mu}(\mathbf{z}_0)}{2N}. \quad (31)$$

Therefore the properties of local minima w.r.t.  $B$  depend only on the relative distances between the eigenvalues and on the problem size  $N$ .

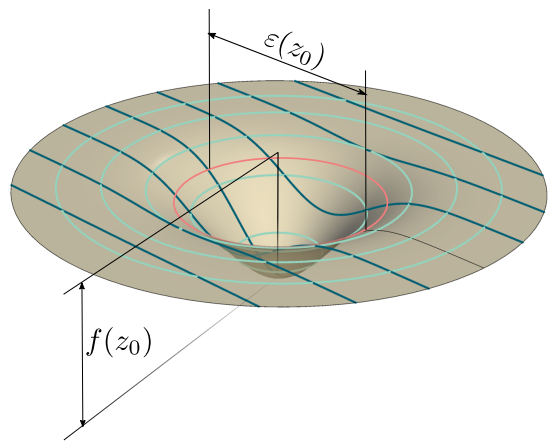


FIG. 3: Schematic visualization of a valley (troughs in higher dimensions not indicated): Driving with  $iC$  (cyan lines), does not change the value of the functional. Driving with  $iB$  is in some sense the ‘orthogonal’ direction. In a valley all  $iB$  trajectories have a local minimum. We identify the size of a valley by region in which the second derivative is positive, here indicated by a red line

### 3. Performance indicators

Valleys have an critical influence on the performance of deep circuit QAOA as they are encompassing attractors and traps for local search routines. Intuitively, a landscape with ‘too many’ valleys, i.e. too many traps, seems to be unfavourable for a good performance. The previous section employs us now with tools for making such a statement more refined: In the following we consider the distribution of valleys with respect to their number, size, and depth. The statistics of these properties allow us then to identify obstacles for local search routines. By this we obtain an accessible performance indicator for deep circuit QAOA.

Recall that the presence of a valley can be attested by the parameter  $\mu(\mathbf{z})$ , where  $\mu(\mathbf{z}) \geq 0$  shows that we have a valley with a radius (in trace distance) that can be estimated by (27). For a given target function  $f: \mathbb{B}^N \rightarrow \mathbb{R}$ , consider the set

$$\Xi_f = \{(f(\mathbf{z}), \mu(\mathbf{z})) \mid \mathbf{z} \in \mathbb{B}^N\}. \quad (32)$$

From now on, we refer to a density plot of  $\Xi_f$  as the  $\mu$ - $f$  diagram of  $f$ . A lot of quantitative structure of the optimization landscape in state space can be directly observed from such a diagram. Several examples are given throughout this section (see e.g. Figure 4, which provides an example for a favourable landscape).

Relevant question that can be directly answered by looking at a  $\mu$ - $f$  diagram are:

- (i) What is the fraction of points with  $\mu > 0$ ? This will give us an estimate on the total amount of valleys.

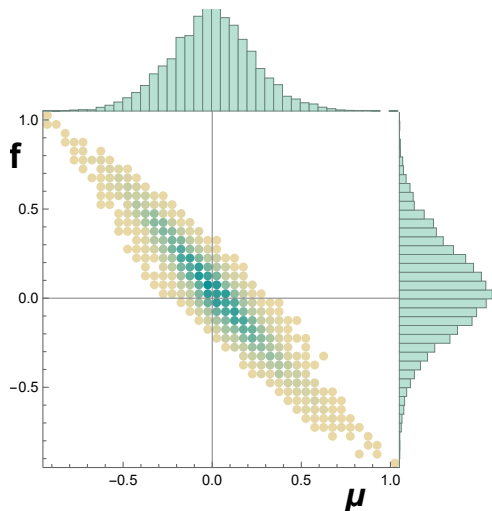


FIG. 4: A  $\mu$ - $f$  diagram for a random instance of QUBO on 13 qubits. This diagram unveils a optimization landscape that is favourable for QAOA

- (ii) Are there correlations between the radius of a valley and its depth? Are the largest valleys also the deepest?
- (iii) Is there a separation between small and large valleys? Are large valleys less likely than small ones?

Quantitative answers to these questions allow us to estimate whether a landscape is in principle favourable or unfavourable for local search routines.

Generally a landscape with only few valleys (i) can be considered as favourable. Non-primitive routines for local search include subroutines for jumps that allow to escape a local trap and search for an optimum elsewhere. This can however only be performant if there are not too many traps. Without further structure given, we will assume that valleys with a large radius are more likely to attract a local search routine. Landscapes whose largest valleys are also the deepest ones (ii) can be considered as favourable, since here a local search is likely to find the global minimum of  $f$ . One central aspect within the fine tuning of a local search routine is to adjust sizes of local steps and jumps. Here statistical information about the valley sizes (iii) can be very useful. In a favourable case the most valleys are small and shallow and only few valleys (including those we are looking for) are large and deep. Taking step sizes and jump sizes big enough will then allow us to fine tune a local search that effectively ignores small valleys and only gets attracted by large ones. In conclusion we will consider landscapes as favourable if the largest valley is also the deepest and the distribution of  $\mu$  and  $f$  thins out for increasing  $\mu$  and decreasing  $f$ , i.e. to the low-right corner of the  $\mu$ - $f$  diagram.

In the sense that it indicates the existence of performance obstacles, we mark the  $\mu$ - $f$  diagram of a target objective  $f$  as a two dimensional performance indicator.

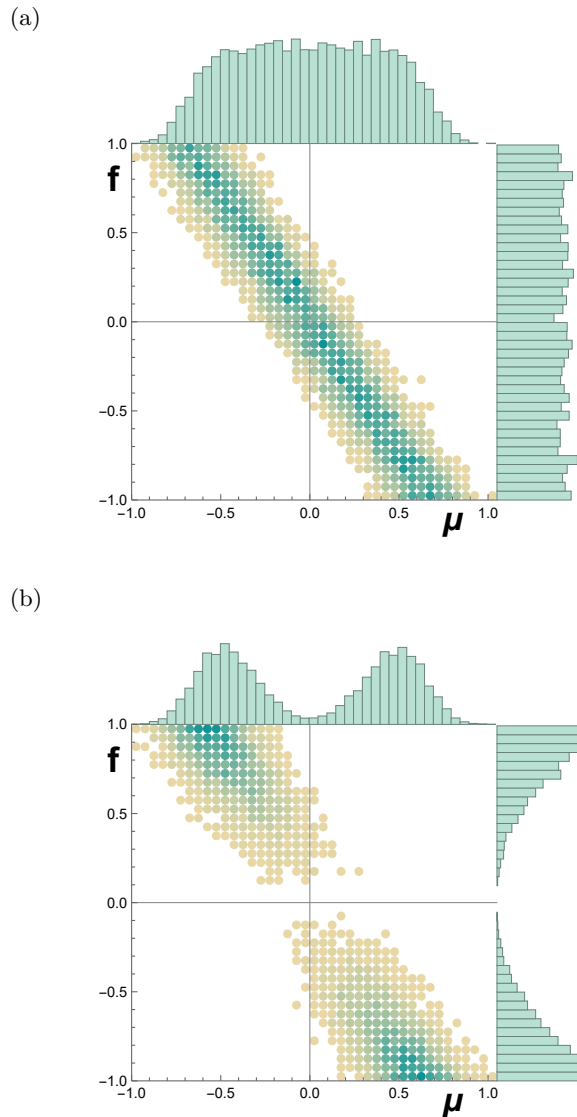


FIG. 5: Unfavourable instances from a randomly drawn  $f$ ,  $10^{13}$  points. The values of  $f$  are distributed with support on  $[-1, 1]$  and (a) uniform randomly distributed and (b) distributed with respect to a 'camel back' distribution.

Here we want to highlight once more that the  $\mu$ - $f$  diagram only depends on data that can be obtained from only looking at classically accessible properties of  $f$  on strings  $z$  (the value of  $f$  and its average on nearest neighbors). Hence statistical distribution properties can be estimated by a simple sampling of  $f$  and  $\mu$  over a set of randomly drawn strings.

On a more refined level, the task of assessing the unfavorability of a landscape translates into the task of estimating a tail distribution. This is a central task within the mathematical field of risk management<sup>22</sup> and many of the statistical methods developed there can be translated to our problem. At this point we however leave

a detailed analysis and application of those methods for future work and restrict for the moment to the provision of examples.

#### 4. Examples

A central question for the assessment of the perspectives of QAOA is to spot instances and problem classes in those an algorithm has a chance for a good performance. In general one has however to expect the existence of 'no free lunch'- theorems implying that most instances will not perform.

We immediately observe such a behaviour when considering objectives  $f$  in which the values of  $f$  are distributed without paying attention to the topology of  $\mathbb{B}^N$ .

Examples are given in Figure 5 here we first generated the values of  $f$  according to a distribution function, and then assigned them with uniform randomness to bit strings. In the first example  $f$  is also uniformly distributed over the interval  $[-1, 1]$  leading to an unfavourable landscape in which the valley sizes are uniformly distributed, as well. In the second example from Figure 5 we distributed the values of  $f$  with respect to a 'camelback' distribution. Here a 'no free lunch' behaviour clearly reveals. Eventhough, the values of  $f$  have a certain thin-tail behaviour (see the drop of density towards  $\pm 1$ ) the distribution of  $\mu$  concentrates around those points. This means that the global minimum has no distinct statistical behaviour with respect to a substantial amount of the local traps.

This situation changes when we consider random instances of QUBO, i.e.

$$f(\mathbf{z}) = \sum_{i,j} z(i)M_{ij}z(j) \quad (33)$$

generated from a randomly chosen hermitian matrix  $M$  with unit norm. Here we have that the value of  $f$  on neighbouring strings stands in a relation. The  $\mu$ - $f$  diagram is shown in Figure 4. Here we have a thin tail and hence a favourable landscape. In correspondence we also see from our numerical studies that already a local search with a simple downhill simplex method performs better on those instances. We expect that this tail behaviour can be explained by employing the central limit theorem. We however leave a full proof for future work. When going through the catalogue of special classes of pseudo Boolean functions<sup>23</sup> one can immediately spot further classes that admit a favourable landscapes. One of those are functions that are zero on almost all strings, and negative on only very few. Think for example on a SAT problem with only few feasible points. Remarkably those are in close correspondence to the 'find the marked entry in a database' problem Grovers search algorithm<sup>24</sup> solves with a proven quantum speedup.

More examples of  $\mu$ - $f$  diagrams can be found in the next section where we report on our numerical studies

performed on certain MAXCUT and MAX-3-SAT instances.

## V. NUMERICAL RESULTS

In this section we evaluate our performance indicators for well-known problem instances. During the last years MAXCUT has established itself as the prototypical benchmarking problem for quantum algorithms. Accordingly, there is various work on MAXCUT problem instances in particular in connection to the QAOA<sup>2,25</sup>. Furthermore, we consider prototypical MAX-3-SAT problems and refer to [26] discussing the defined clause density in the light of our approach. In the following, we evaluate  $\mu$ - $f$  statistics for instances of both problem classes.

Since we aim to discuss deep-circuit QAOA, we will use a simple local search routine: a layer-by-layer optimization, which iteratively adds layers  $(\beta, \gamma) \in [-\delta, \delta]^2$  optimized over a  $k \times k$  mesh. This approach offers several advantages: First, one can rebuild all results quite easily. Second, this method is suitable for and allows for comparison of various problem instances. We further relate the  $\mu$ - $f$  statistics to a promising step size  $\delta$  in the local search routine.

### 1. MAXCUT

Consider a graph  $G = (V, E)$  with vertex set  $V$  and edge set  $E$ . We search for a partition of the vertex set  $V = S \dot{\cup} T$  with maximal number of edges between these two vertex sets  $S$  and  $T$ . We identify every vertex with a bit  $z_i$  and its value is set to one, if the vertex is in  $S$  and zero if it is in  $T$ . This said, the cost function for MAXCUT is given by

$$f(\mathbf{z}) = \sum_{i,j=1}^N \omega_{ij}(z_i - z_j)^2,$$

where  $(\omega_{ij})$  is the adjacency matrix. Note the degeneracy stemming from the symmetry of  $f(\mathbf{z})$  under exchange of bits. Applying the encoding  $z_i \mapsto (1 - \sigma_z^{(i)})/2$ , we obtain the objective Hamiltonian

$$H = \frac{1}{2} \sum_{i,j=1}^N \omega_{ij}(1 - \sigma_z^{(i)}\sigma_z^{(j)})$$

which is obviously a QUBO instance.

We choose to analyze two prototypical examples of 3-regular graphs with 6 vertices, one being the complete bipartite graph  $K_3^2$ , the other being the prism. The two graphs together with their corresponding  $\mu$ - $f$  diagrams are displayed in Figure 6.

Here, we already see distinct properties of both graphs. Mainly, one recognizes a symmetric density distribution of local minima ( $\mu > 0$ ) and local maxima ( $\mu < 0$ ) only



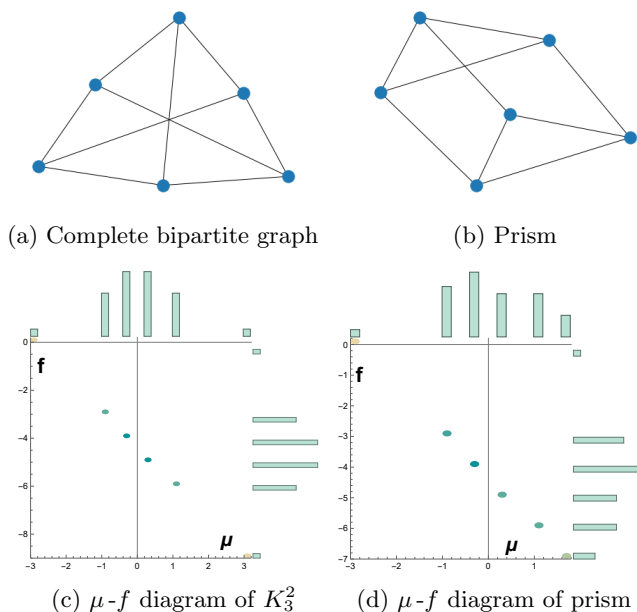


FIG. 6: Examples of 3-regular graphs with corresponding  $\mu$ - $f$  diagrams.

for  $K_3^2$  and one isolated global minimum and maximum, respectively. In contrast, the prism provides denser packing of local minima and one highly isolated global maximum. This is reflected in different optimal step sizes as shown in Figure 7. However, in both cases the diagrams clearly indicate an anticorrelation between  $f$  and  $\mu$  values. In particular, the maximum of  $\mu$  corresponds to the minimum of  $f$  and vice versa. Thus, minimizing  $f$  is equally accomplished by searching for the biggest valley.

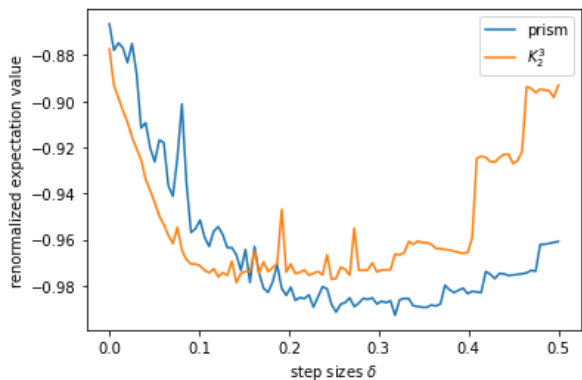


FIG. 7: Sample of different step sizes for  $k = 20$  and  $p = 25$  with downhill algorithm.

We observe that for  $p = 25$  both graphs indeed admit different optimal step sizes  $\delta$ . In each case, however, the approximation quality decreases for step sizes that are too small ( $\delta < 0.1$ ) or too large ( $\delta > 0.4$ ). For small step sizes, two explanation are plausible: First, the instance could suffer from reachability deficiencies, i.e.,

too small parameters do not suffice to get close to any optimal state. Second, the method could get stuck in non-optimal local minima since the steps are too small to escape an attracting  $\varepsilon$ -valley (see Section V.2). For large step sizes, we infer that the  $m \times m$  mesh is too coarse to find the optimal parameters. Additionally, the observed sharp peaks could result from periodicities in the parameter landscape, which cause the algorithm to get caught in a non-optimal state.

We further calculate the optimal step size for circuit depths up to  $p = 500$  and compare the performance of these optimized QAOA instances to a naive QAOA instance with constant small angles. Figure 8 shows the fast convergence of the downhill method after a few steps. In contrast, the naive instance struggles to approximate any ground state even for large  $p$ . Figure 9 shows the

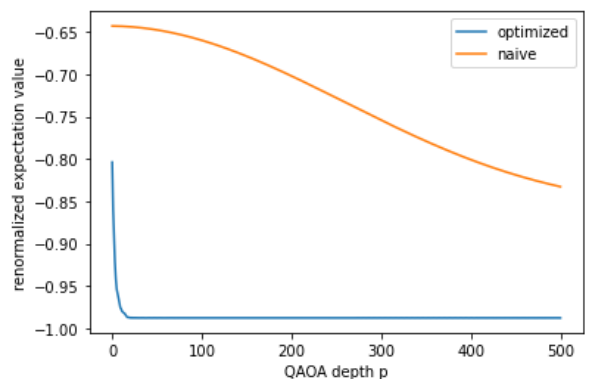


FIG. 8: Comparison of the naive QAOA instance and the optimized QAOA routine with downhill algorithm for deep circuits. The naive QAOA routine uses constant parameters  $\beta, \gamma \equiv 1/500$ .

bit string distribution after applying the optimized and the naive QAOA, respectively. The better approximation quality of the optimized QAOA reflected in the high amplitudes of the optimal computational states. In the Appendix, we show an evolution of the layer-by-layer optimization for increasing  $p$ . There one sees a deformation of the landscape during the process which matches the observations from [25] about reachability for different  $p = 1$ . In Figure 9 we observe that the optimized QAOA as well as naive QAOA approximate a uniform superposition of all optimal computational basis states. Recall our discussion in Section IV.2 about the differences on the goal of an algorithm in trace distance; a priori it is unclear, whether an algorithm drives into the superposition of all computational basis states or stays in a proper subset of them. In the general QAOA algorithm it is to our knowledge unclear, if one could control this process.

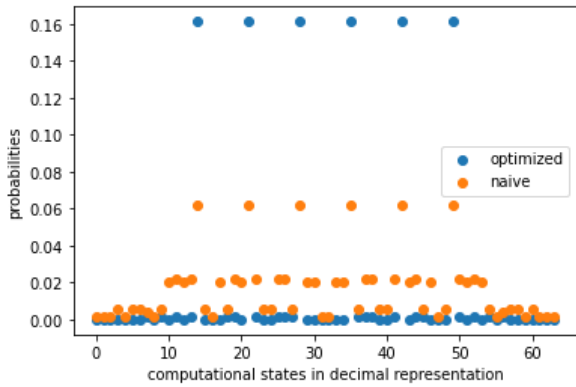


FIG. 9: Comparison of the naive QAOA and the optimized QAOA routine with downhill algorithm for deep circuits.

## 2. Example of trap behaviour

In this section, we numerically investigate what happens if the step size  $\delta$  is so small that

$$\| |z_0\rangle\langle z_0| - e^{-i\beta B} e^{-i\gamma C} |z_0\rangle\langle z_0| e^{i\gamma C} e^{i\beta B} \|_1 \leq \varepsilon \quad (34)$$

holds for a trap  $|z_0\rangle\langle z_0|$ . We consider again the prism as shown in Figure 6. Here, the bit string 101100 with

$$f(101100) = -5$$

corresponds to a local minimum which is not a global one, hence a trap. We calculate that  $\|[B, [B, C]]\|_\infty \leq 41$  and  $2 \cdot N \cdot \mu(101100) = 4$ . Thus, by (27)  $\varepsilon_{101100} \leq 0.1$ . Note that, at least for this MAXCUT instance, for

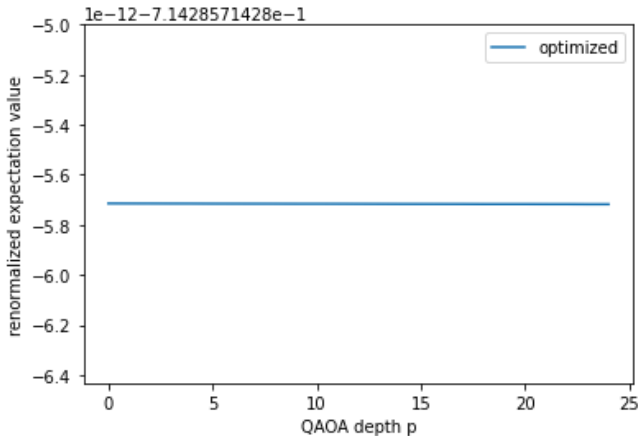


FIG. 10: The expectation value in dependence of the depth  $p$  for the downhill algorithm with  $-0.03 \leq \beta \leq 0.03$  and  $-0.015 \leq \gamma \leq 0.015$ .

every computational basis state  $|z\rangle\langle z|$  the quantity  $\text{tr}(|z\rangle\langle z|[B, [B, C]])$  is integer-valued and does not exceed  $\|[B, [B, C]]\|_\infty$ . Therefore,  $\varepsilon$  is properly estimated

by the latter. We then derive ranges for  $\beta$  and  $\gamma$  so that (34) holds. Now we apply the downhill algorithm with parameters drawn from this rectangle. The result shown in Figure 10 confirms the expected trap behaviour discussed in Section IV: due to the small step size the algorithm is not able to leave the local minimum.

In Figure 11 we display a two-dimensional section of the state space landscape in polar coordinates around the trap  $\xi := |101100\rangle\langle 101100|$  where the radius and angle coordinates correspond to  $\beta$  and  $\gamma$ , respectively. One clearly sees that the functional is invariant along all curves where  $\beta = \text{const}$ .

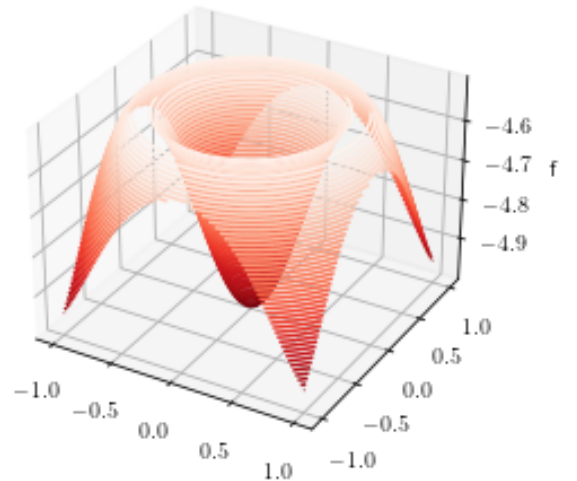


FIG. 11: State space landscape around the trap  $\xi$  in polar coordinates.

Since applying  $U_C$  does not affect the trap state  $\xi$ , we further investigate the single action of  $U_B(\beta)$  with varying parameter  $\beta$  (see Figure 12).

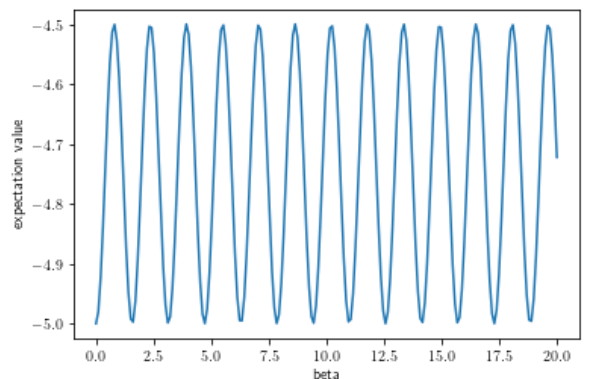


FIG. 12: The expectation value in dependence of only  $\beta$  steps starting in the local minimum  $\xi$ .

Here we observe, that the expectation value, as a function of the parameter  $\beta$ , becomes periodically. Numer-

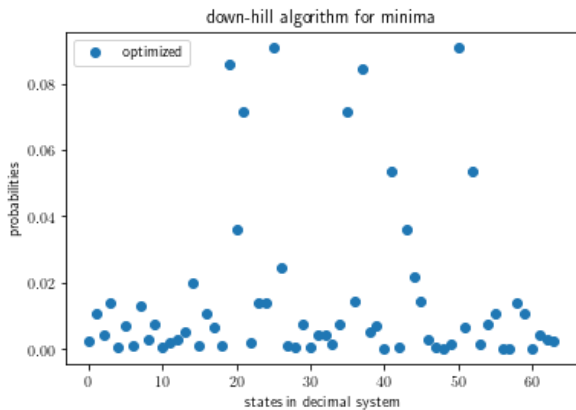


FIG. 13: The probability distribution after moving one step in  $iC$ ,  $iB$ , and  $[B, C]$  direction from  $\xi$ , respectively.

ically, the same behavior can be witnessed when small steps in  $iC$  direction alternate with actions of  $U_B(\beta)$ .

Hence, the only option is to choose a *new* direction in the Lie algebra in order to escape from the trap. Here we use the commutator of  $B$  and  $C$ .

As Figure 13 shows moving along the  $[B, C]$  direction allows us to escape from the trap  $\xi$ , otherwise the probability would still be concentrated at the trap.

### 3. Random MAX-3-SAT

As a second problem class, we consider MAX-3-SAT. Its goal is to find a bit string that satisfies the maximal number of some clauses consisting of three literals. For that purpose, we created random instances with  $m = 6, 9, 12, 18$  clauses on 6 (qu)bits and look at their  $\mu$ - $f$  diagrams (Figure 14)

The overall picture is quite different in this problem class. The diagrams remind of an extraction from the unfavorable instance of a uniform randomly distributed function in Figure 5. What strikes the eye is that with increasing number of clauses the deepest valleys are no longer guaranteed to be the largest. In this case, the approach of a constant step size depending on the size of the valley becomes futile. Another interesting point is, that the ‘gap’ between the lowest value and the second lowest gets smaller with more clauses. In addition, a larger amount of clauses leads to more local minima. Therefore, the QAOA approximately reaches the neighborhood of the lowest value very good, without taking the lowest value. From this perspective, it seems to be natural, that one observes reachability deficits like [26].

In terms of plotting the renormalized expectation value against the step size for circuit depth  $p = 25$  in Figure 15 this translates to two insights:

1. Increasing the number of clauses decreases approximation quality of the QAOA, resembled in an overall increase of the expectation value.

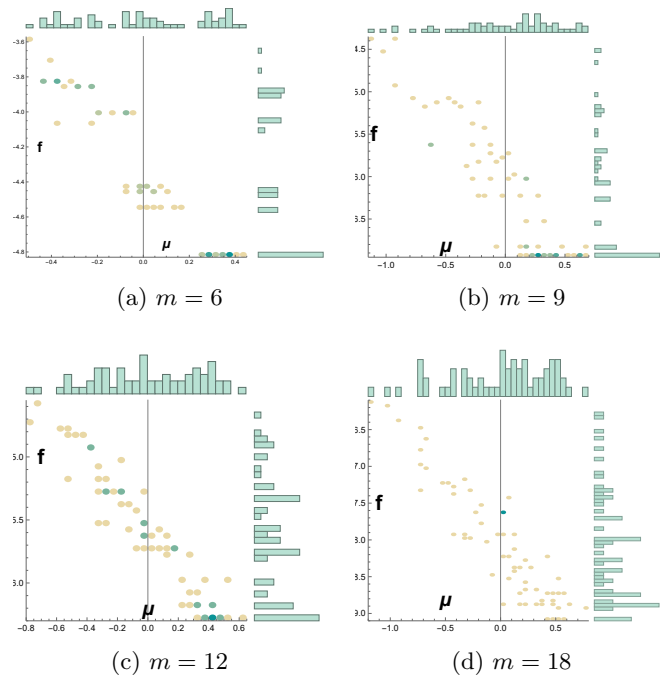


FIG. 14:  $\mu$ - $f$  diagram for random weighted MAX-3SAT instances with  $m$  clauses

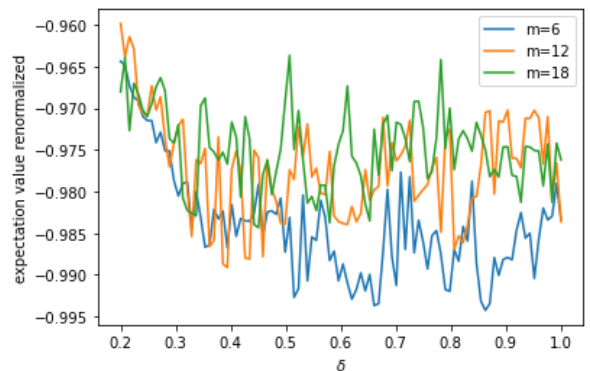


FIG. 15: The step size analysis for  $0.2 \leq \delta \leq 1$  and number of clauses  $m = 6, 12, 18$  ( $p = 25$ ).

2. The diagram does not suggest a preferred regime of step size indicating that the concept of a fixed step size for this problem class is to be refused.

We guess from Figure 15 optimal step sizes for these three examples of the number of clauses. The results of QAOA instances with varying depth  $p$  and respective optimal step sizes are shown in Figure 16.

In Figure 17 we observe that the optimal state’s amplitude does not sufficiently tower above the other amplitudes to reliably identify the optimal bit string in a measurement. This emphasizes that even though the algorithm quickly delivers nearly optimal expectation val-

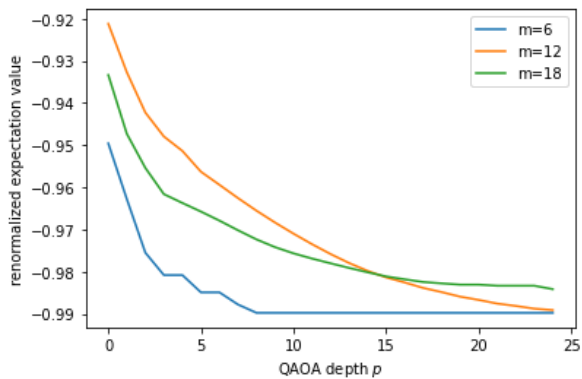


FIG. 16: The optimal expectation value achieved by QAOA instances with  $p = 0, \dots, 25$  for MAX-3-SAT with  $m = 6, 12, 18$ .

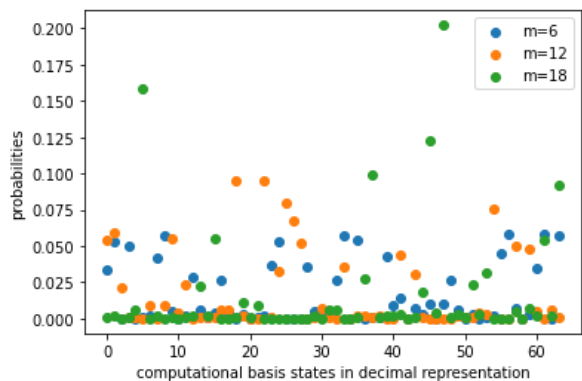


FIG. 17: The probability distribution for MAX-3-SAT with  $m = 6, 12, 18$  after applying the QAOA with depth  $p = 25$  and optimal step size. The computational basis states are labeled by decimal representation.

ues it merely slowly converges to the optimal state.

## VI. OUTLOOK AND CONCLUSION

This work is done under the impression that technological advances of the NISQ era might reach a next stage in a not too far future. For this we share the aspirations that quantum computing with deep circuits will become practically feasible. In this regime the quantum-classical ansatz of variational quantum computing will likely keep its popularity. Estimating perspectives of practical applicability, spotting new obstacles, and finding promising problem classes is therefore a relevant quest that can already be started today.

By this work we contribute to the collection of methods, tools, and structural insights that will hopefully lead to a better understanding on the QAOA practically fails in many examples and when it could in principle work.

As we have seen, regarding optimization landscapes from a state space perspective allows for a clear analysis

that reveals rich but still accessible mathematical structures. This has to be seen in clear contrast to the, in some extend, more often employed perspective on optimization landscapes in the parameter space of  $(\beta, \gamma) \in \mathbb{R}^{2p}$ . The mapping from  $(\beta, \gamma) \in \mathbb{R}^{2p}$  does not really respect the natural topology of the problem. Several, apparently different, local minima and traps in parameter space could for example correspond to one and the same local minimum in state space. In this sense obstacles that are spotted in the state space picture give us a clear hint towards the persistent geometric core of the underlying problem.

We expect that the analysis of the  $\mu$ - $f$  diagrams, which we introduced as performance indicators, will turn out as a useful tool for future research. By considering only few basic examples, we merely scratched on the surface of its applicability. Analyzing these indicators and evaluating their impact for practical problem instances will be an essential task for future research. At the moment we are evaluating the distributions of traps for problem instances coming from annual MAXSAT Evaluations benchmarking contest<sup>27</sup>. We leave the results of this for a future publication.

From the results we have seen so far, it becomes however already clear that there will be no universal applicability of QAOA in deep circuits. We see that problem instances that avoid unfavourable landscapes must have a specialized underlying structure and are presumable rare. This is totally in line to the typical observation that no method ever gives a free lunch.

Lastly, we have to point out that many further aspects that influence the performance of a local search have been neglected in this work. This especially includes the actual circuit depth required for approximating the solution of a problem up to a convincing ratio. For local search routines this depth can be highly problem specific and might drastically vary with respect to the explicit method in use. Finding good routines will most likely demand a lot of explicit feature engineering. Even though we found some promising tiny and simple examples in our numerical studies, a conclusive assessment of instances with favourable landscapes can very likely reveal further obstacles. At this point the results of our work can only make a beginning.

## Acknowledgments

We thank Daniel Burgarth, Tobias J. Osborne, Antonio Rotundo, Bence Marton Temesi, Arne-Christian Voigt, Sören Wilkening, and Reinhard F. Werner for helpful discussions. GK acknowledges financial support by the DAAD and IIT Indore (Kapil Ahuja) for a guest stay. LvL and RS acknowledge financial support by the Quantum Valley Lower Saxony. RS acknowledges financial support by the BMBF project ATIQ. TZ acknowledge financial support by the BMBF project QuBRA.



- <sup>1</sup>M. Cerezo, A. Arrasmith, R. Babbush, S. C. Benjamin, S. Endo, K. Fujii, J. R. McClean, K. Mitarai, X. Yuan, L. Cincio, and P. J. Coles, *Nature Reviews Physics* **3**, 625 (2021).
- <sup>2</sup>E. Farhi, J. Goldstone, and S. Gutmann, A quantum approximate optimization algorithm (2014), [arXiv:1411.4028 \[quant-ph\]](https://arxiv.org/abs/1411.4028).
- <sup>3</sup>M. P. Harrigan *et al.*, *Nature Physics* **17**, 332 (2021).
- <sup>4</sup>M. Willsch, D. Willsch, F. Jin, H. D. Raedt, and K. Michielsen, *Quantum Information Processing* **19**, 197 (2020).
- <sup>5</sup>P. Vikstål, M. Grönkvist, M. Svensson, M. Andersson, G. Johansson, and G. Ferrini, *Physical Review Applied* **14**, 034009 (2020).
- <sup>6</sup>D. Lykov, J. Wurtz, C. Poole, M. Saffman, T. Noel, and Y. Alexeev, Sampling frequency thresholds for quantum advantage of quantum approximate optimization algorithm (2022), [arXiv:2206.03579 \[quant-ph\]](https://arxiv.org/abs/2206.03579).
- <sup>7</sup>J. Lee, A. B. Magann, H. A. Rabitz, and C. Arenz, *Physical Review A* **104**, 032401 (2021).
- <sup>8</sup>The original QAOA is formulated for maximization tasks; here  $B$  is defined with the opposite sign.
- <sup>9</sup>S. Endo, S. C. Benjamin, and Y. Li, *Physical Review X* **8**, 031027 (2018).
- <sup>10</sup>L. Egan, D. M. Debroy, C. Noel, A. Risinger, D. Zhu, D. Biswas, M. Newman, M. Li, K. R. Brown, M. Cetina, and C. Monroe, *Nature* **598**, 281 (2021).
- <sup>11</sup>M. Larocca, P. Czarnik, K. Sharma, G. Muraleedharan, P. J. Coles, and M. Cerezo, Diagnosing barren plateaus with tools from quantum optimal control (2021), [arXiv:2105.14377 \[quant-ph\]](https://arxiv.org/abs/2105.14377).
- <sup>12</sup>J. R. McClean, S. Boixo, V. N. Smelyanskiy, R. Babbush, and H. Neven, *Nature Communications* **9**, 4812 (2019).
- <sup>13</sup>X. Ge, R.-B. Wu, and H. Rabitz, The optimization landscape of hybrid quantum-classical algorithms: from quantum control to nisq applications (2022), [arXiv:2201.07448 \[quant-ph\]](https://arxiv.org/abs/2201.07448).
- <sup>14</sup>This is clear for finite circuits, for infinite circuits the proper limits have to be taken into account.
- <sup>15</sup>On an abstract level we can consider  $G$  as a subgroup of  $GL(n, \mathbb{C})$ . Here Cartan's theorem on closed-subgroups<sup>28</sup> states that the embedding of  $G$  into the smooth structure of  $GL(n, \mathbb{C})$  will give us a consistent smooth structure on  $G$  itself.
- <sup>16</sup>S. Lloyd, *Physical Review Letters* **75**, 346 (1995).
- <sup>17</sup>D. Deutsch, A. Barenco, and A. Ekert, *Proceedings: Mathematical and Physical Sciences* **449**, 669 (1995).
- <sup>18</sup>M. E. S. Morales, J. D. Biamonte, and Z. Zimborás, *Quantum Information Processing* **19**, 291 (2020).
- <sup>19</sup>C. Altafini, *Journal of Mathematical Physics* **43**, 2051 (2002).
- <sup>20</sup>A. A. Agrachev and Y. L. Sachkov, *Control theory from the geometric viewpoint*, Vol. 2 (Springer Science & Business Media, 2004).
- <sup>21</sup>J. R. Shewchuk, *An Introduction to the Conjugate Gradient Method Without the Agonizing Pain*, Tech. Rep. (USA, 1994).
- <sup>22</sup>J. S. Baker and S. K. Radha, Wasserstein solution quality and the quantum approximate optimization algorithm: A portfolio optimization case study (2022), [arXiv:2202.06782 \[quant-ph\]](https://arxiv.org/abs/2202.06782).
- <sup>23</sup>Y. Crama and P. L. Hammer, *Boolean Functions Theory, Algorithms, and Applications* (Cambridge University Press, 2011).
- <sup>24</sup>L. K. Grover, A fast quantum mechanical algorithm for database search (1996), [arXiv:9605043 \[quant-ph\]](https://arxiv.org/abs/9605043).
- <sup>25</sup>Z. Wang, S. Hadfield, Z. Jiang, and E. G. Rieffel, *Physical Review A* **97**, 022304 (2018).
- <sup>26</sup>V. Akshay, H. Philathong, M. E. S. Morales, and J. D. Biamonte, *Physical Review Letters* **124**, 090504 (2020).
- <sup>27</sup>Maxsat evaluations (2006-2022), <https://maxsat-evaluations.github.io/>.
- <sup>28</sup>J. M. Lee, *Introduction to Smooth Manifolds*, Vol. 218 (Springer New York, NY, 2003).
- <sup>29</sup>R. Zeier and T. Schulte-Herbrüggen, *Journal of mathematical physics* **52**, 113510 (2011).
- <sup>30</sup>R. Zeier and Z. Zimborás, *Journal of Mathematical Physics* **56**, 081702 (2015).
- <sup>31</sup>Z. Zimborás, R. Zeier, T. Schulte-Herbrüggen, and D. Burgarth, *Physical Review A* **92**, 042309 (2015).

## VII. APPENDIX

### 1. Universality of the generic QAOA Lie algebra

*Proof of Theorem 1.* Given Hermitian operators  $B$  and  $C$  on a (finite dimensional) Hilbert space  $\mathcal{H}$ , under what conditions is the generated Lie algebra  $\text{Lie}(iB, iC)$  equal to  $\mathfrak{su}(\mathcal{H})$ ? This question is particularly important in the field of *control theory* and has, for example, been looked at in<sup>19,29–31</sup>. We will use the sufficient condition in<sup>19</sup> (Theorem 2) stating that if  $C$  is strongly regular (which is equivalent to our assumptions (a) and (b)<sup>19</sup>) and if the graph  $\mathcal{G}$  is connected (see below), then  $\mathfrak{g}(B, C) = \mathfrak{su}(\mathcal{H})$ . Of course,  $G = \text{SU}(\mathcal{H})$  and  $\mathfrak{g}(B, C) = \mathfrak{su}(\mathcal{H})$  are equivalent.

The graph  $\mathcal{G}$  of an operator  $B$  is defined w.r.t. a basis  $\{|s\rangle \in S\}$  as follows: The vertices of  $\mathcal{G}$  are the different basis labels  $s \in S$  and there is an oriented edge joining  $s$  and  $s'$  if  $\langle s|B|s'\rangle \neq 0$ . The basis we choose is the standard one, i.e., our vertices are bit strings of length  $N$ . Since  $B$  is Hermitian, there is an edge joining  $s$  and  $s'$  if and only if there is an edge joining  $s'$  and  $s$ , i.e., the graph  $\mathcal{G}$  is effectively undirected. It remains to show that the graph  $\mathcal{G}$  of  $B$  is connected, i.e., that all  $s$  and  $s'$  can be joined by a composition of edges. To get started, we look at

$$\langle s|B|s'\rangle = \sum_{j=1}^N \langle s|f_j(s')\rangle$$

where  $f_j$  flips the  $j$ -th bit, e.g., if  $N = 3$ , then  $f_2(100) = 110$ . This is zero if and only if each summand is zero, which happens precisely if the bit strings  $s$  and  $s'$  differ in more than two positions, i.e., have a *Hamming distance* of more than one. This shows that in the graph  $\mathcal{G}$  of  $B$ , whose vertices are bit strings, there is an edge between two bit strings if and only if their Hamming distance is one. This makes it obvious that the graph is connected. For example in the case  $N = 3$  we can go from 000 to 111 in the following way  $000 \rightarrow 001 \rightarrow 011 \rightarrow 111$ .  $\square$

### 2. Local picture of steps

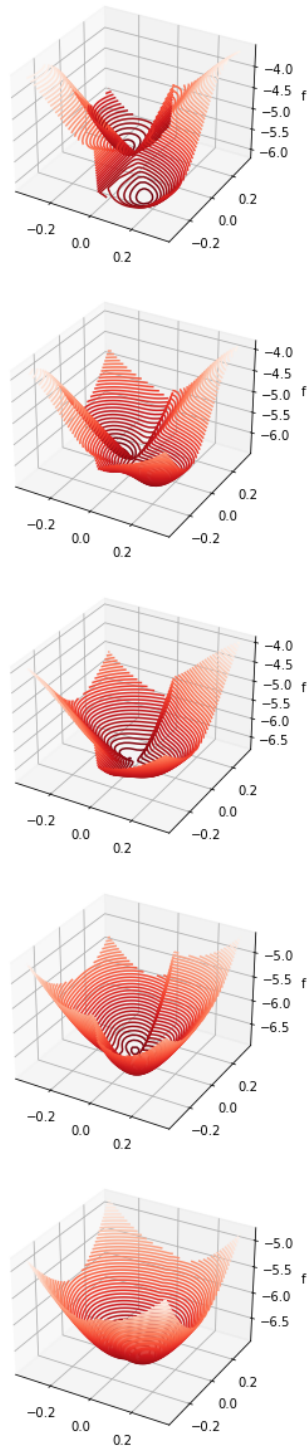


FIG. 18: Evolution of a layer by layer optimization for different  $1 \leq p \leq 20$  with optimal step size (here for prism).